Engineering Structures 275 (2023) 115108

Contents lists available at ScienceDirect

Engineering Structures

journal homepage: www.elsevier.com/locate/engstruct

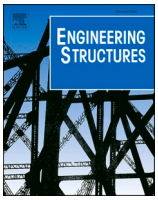

Experimental and numerical simulation study on mechanical properties of fiber-reinforced plastic seismic isolator

Hao Wang [a], Haoran Mu [b], Xiaoxia Guo [b], Yunfei Zhang [b], Haowei Ji [b], Chao Luo [a,*], Huaiping Feng [a,*], Donglin Liu [b]

[a] State Key Laboratory of Mechanical Behavior and System Safety of Traffic Engineering Structures, Shijiazhuang Tiedao University, Shijiazhuang 050043, China
[b] School of Civil Engineering, Shijiazhuang Tiedao University, Shijiazhuang, Hebei Province 050043, China

ARTICLE INFO

Keywords:
FRP seismic isolator
Low-cost isolator
Mechanical property tests
Isolator's stress distributions

ABSTRACT

Seismic isolators are widely used in the field of seismic mitigation. But the disadvantage of the high cost limits the promotion of seismic isolators in underdeveloped areas. Therefore, the development of a new type of low-cost seismic isolator will facilitate the application of seismic isolation technology. This paper proposes a fiber-reinforced plastic (FRP) seismic isolator with cost-effective and stable mechanical performance features, which uses a synthetic material of alkali-free fabrics and vinyl resin instead of the steel plate in the traditional laminated isolator. The design and manufacturing process of the bearing makes it have higher stability and integrity than the traditional bearing. A series of mechanical properties tests were conducted to investigate the mechanical behavior of the FRP seismic isolator and to determine the boundary properties of the FRP seismic isolator. The stress distributions inside the FRP seismic isolator are analyzed detailly by the finite element model. The effects of changing the plane size of the FRP seismic isolator and the plate/rubber thickness ratio (P/RTR) on the isolator performance were studied to provide technical support for the subsequent design and manufacture of FRP seismic isolators. The experimental and numerical analyses show that the FRP seismic isolators developed in this paper have good performance and are beneficial for application in low-rise building structures.

1. Introduction

At present, seismic isolators are widely used in the field of seismic mitigation, effectively reducing the seismic responses of various structures and the impact of hazards. However, the seismic isolator has the disadvantage of high cost and is more challenging to apply and promote in underdeveloped areas. So developing a low-cost seismic isolator has practical significance.

Many scholars have studied low-cost seismic isolation techniques, and these isolation devices can be concluded into three main categories [1]: sliding seismic isolation, rocking seismic isolation and elastomeric seismic isolation. There are two main types of sliding seismic isolation. One type of sliding seismic isolation [2,3] dissipates seismic energy by sliding the planes or spheres in the isolator under the excitation of an earthquake. The friction isolation is generally made of steel plates, natural stone, and Teflon sheets, which are easy to obtain and durable. Another type of sliding seismic isolation [4,5] dissipates seismic energy by friction between granules in a sand layer, sand-rubber layer or stone layer laid at the bottom of the structure. So they have the advantages of favourable seismic isolation effects and a wide range of applicable seismic frequencies. But sliding seismic isolation is relatively challenging to restore after an earthquake. The rocking seismic isolation [6,7] usually uses rolling rods or rolling balls, which will have the self-return capability if they are laid on a sloping surface. Still, they have problems of stress concentration and less energy dissipation capacity, and they require maintenance to maintain normal operation throughout the working period. The elastomer seismic isolation interconnected rubber layers and layers of steel or fiber through a special process. Although the elastomer seismic isolators [8] are relatively expensive to produce, they have the advantages of good resilience and good seismic isolation effect. Therefore, the elastomer seismic isolators have a broad application prospect.

Due to the elastomeric isolation's advantages, many scholars have conducted research on low-cost elastomeric seismic isolators. In 1999 Kelly [9] proposed using fiber-reinforced material to replace steel plates in the elastomer seismic isolator. Tsai [10,11] theoretically deduced the

* Corresponding authors.
E-mail addresses: luochao@stdu.edu.cn (C. Luo), fenghuaiping@stdu.edu.cn (H. Feng).

https://doi.org/10.1016/j.engstruct.2022.115108
Received 3 April 2022; Received in revised form 11 August 2022; Accepted 7 October 2022

theoretical stiffness and ultimate deformation capacity of the fiber-reinforced elastomeric isolator. Angeli et al. [12] proposed an analytical model of a carbon-fiber-reinforced rectangular isolator based on Kelly's study, considering the reinforcing material's flexibility and the rubber's compressibility. Through experimental studies, Li et al. [13] verified the feasibility of steel meshes as stiffening plates. Mordini et al. [14] analyzed the mechanical properties of the glass-fiber-reinforced elastomeric isolators. The application of the glass fiber seismic isolators on storage tanks showed significant seismic isolation effects. Russo et al. [15] designed different characteristics of fiber-reinforced elastomeric isolators, including different neoprene types, layouts of carbon fiber fabrics, shape factors and aging conditions. Tan et al. [16] designed a simple bearing with unsaturated polyester fiber-reinforced plastic plates and verified that the proposed bearings could be used as the base-isolation devices for low-cost housing. Toopchi-Nezhad [17] established finite element models of bonded and unbonded elastomeric isolators. The fiber-reinforced plate of the unbonded isolator needed to bear less tensile stress; the bonded isolator did not slip and can provide tension between the superstructure and foundation beam. Habieb et al. [18–20] proposed an Abaqus element model suitable for simulating unbonded fiber reinforced elastomeric isolator (UFREI) and fiber reinforced elastomeric isolators were applied to a masonry church to study the effects of seismic isolation. Numerical results show that the damage in masonry churches can be significantly reduced by inserting UFREIs in case of moderate earthquakes. The UFREIs-SMA wires with a specific pre-strain exhibit better seismic isolation in case of strong earthquakes. Niel C et al. [21] proposed the partially bonded fiber-reinforced elastomeric isolator, which can transmit certain tensile force between upper and lower support to reduce the possibility of isolators' slipping under vertical tensile conditions. Moona et al. [22] found that bonded fiber-reinforced elastomeric isolators have better mechanical performances than laminated steel plate rubber bearing. The scholars above expanded the selection of fiber-reinforced materials and proved fiber-reinforced elastomeric isolators' effectiveness through experimental and numerical simulation studies.

The main purpose of this research is to develop a low-cost rubber isolation bearing that can maintain stability without tearing between the stiffener plate and the rubber during strong earthquakes. Therefore, this paper proposes a new fiber-reinforced plastic (FRP) seismic isolator, which uses fiber-reinforced plastic plates to replace steel plates to reduce the cost of the seismic isolator. The FRP seismic isolator is designed with upper and lower sealing plates to increase its stability, and the FRP plate is processed by brushing and other processes to increase the adhesion between the FRP plate and rubber. The fiber-reinforced plastic plate is composed of alkali-free cloth and vinyl resin. In this paper, the mechanical properties of the newly developed bearing are studied by experiments and numerical simulations, which include the following three main steps. Step I: The mechanical properties of the bearings were investigated through tests, which included basic mechanical properties tests, ultimate performance tests, shear strain correlation tests, compressive stress correlation tests, and loading frequency correlation tests. Step II: The stress distributions and values inside the FRP seismic isolator are analyzed detailly by the finite element model. The studied stresses include horizontal normal stresses, vertical normal stresses and interfacial shear stresses. Step III: The effects of changing the plane size of the FRP seismic isolator and the plate/rubber thickness ratio (P/RTR) on the isolator performance were studied. The effect of P/RTR and plane size on the stress values and distribution are analyzed by numerical simulation.

2. Mechanical properties of the FRP plate

The fiber-reinforced plastic plate is made of composite material, which is alkali-free fabrics laminated with vinyl resin, and the alkali-free fabric is made of fiber-glass. The type of resin used in FRP is phenolic epoxy vinyl ester resin, which is made by modifying phenolic epoxy resin with methacrylic acid. In order to meet the mechanical properties requirements of replacing steel plates, the tensile and bending properties of FRP plates are tested. The modality of the tensile test specimen is shown in Fig. 1. The tensile test's procedures are as follows [23]: (1) Measure the width and thickness of the specimens at any three points in the middle range (50 mm $\pm$ 0.5 mm scope, as shown in Fig. 1.) of the specimen, and take the arithmetic mean of three measurements; (2) Clamp the specimen so that the central axis of the specimen is aligned with the centerline of the upper and lower fixture. Load the force continuously at a uniform rate of 2 mm/min until the specimen is damaged and read the damage load value; (3) Install the deformation measuring instrument to measure the elasticity modulus. Apply the initial load on the specimen, which is about 5 % of the damage load. The automatic recording device is available so the test can be loaded continuously; (4) The specimen is invalidated if broken in the fixture or arc, and another specimen is taken to supplement. The photographs of the tensile tests and damaged specimens after the tensile tests are shown in Fig. 2 and Fig. 3, respectively.

Table 1 shows that the maximum, the minimum and the average tensile strengths of the FRP are 370 MPa, 225 MPa and 321 MPa, respectively. The dispersion coefficient of the tensile strength is 0.1469. The maximum, the minimum and the average elasticity modulus of the FRP are 1.9459×10^4 MPa, 1.5023×10^4 MPa and 1.7843×10^4 MPa, respectively. The dispersion coefficient of the elasticity modulus is 0.0875. The maximum, the minimum and the average elongation at break are 3.80 %, 2.86 % and 3.37 %, respectively. The dispersion coefficient of the elongation at break is 0.1075.

The modality of bending specimen is shown in Fig. 4. The specimen's thickness h is 5 mm, and the tolerance of a group of specimens is $\pm$ 0.2 mm. The specimen's width b is 15 mm and the length l is 80 mm. The bending test's procedures are as follows: (1) Number qualified specimens, measure the width and thickness of three points near the center of the specimens span, and take the arithmetic mean of three measurements; (2) Place the specimen in the middle of the support, and the longitudinal direction of the specimen is perpendicular to the upper indenter. The tester is adjusted so that the upper indenter for loading is exactly in contact with the specimen; (3) Apply the initial load on the specimen, which is about 5 % of the damage load; (4) When measuring bending strength and bending stress, the force is loaded continuously at a uniform rate of 10 mm/min until the specimen is damaged, and the damage load or maximum load value is read; (5) A deflection measuring device is installed at the bottom of the specimen to measure the elasticity modulus. Load forces continuously at a loading speed of 2 mm/min; (6) The specimen damaged outside the 1/3 middle range of the specimen should be scrapped. The photographs of the bending test and the damaged specimens after the bending tests are shown in Fig. 5 and Fig. 6, respectively.

Table 2 shows that the maximum, the minimum and the average bending strength of the FRP are 450 MPa, 325 MPa and 377.14 MPa, respectively. The dispersion coefficient of the bending strength is 0.099. The maximum, the minimum and the average bending modulus are 6.65×10^4 MPa, 5.26×10^4 MPa and 5.89×10^4 MPa, respectively. The dispersion coefficient of the bending strength is 0.084.

The FRP can meet the mechanical properties' requirements of the isolator's stiffening material if both the tensile and the bending strengths are beyond 170 MPa [24]. The test results show that the FRP's average tensile and bending strengths are 321 MPa and 377.14 MPa. So the FRP proposed in this paper could be used as stiffening plates instead of steel plates in laminated rubber bearings.

3. Scheme design of the FRP seismic isolator

The FRP seismic isolator is composed of a total of 11 FRP plate layers and 12 rubber layers. The size of the internal FRP plate of the FRP seismic isolator is 240 $\times$ 240 $\times$ 5 mm. The thickness of a single rubber layer is 4 mm, and the total thickness of rubber layers is 48 mm. The

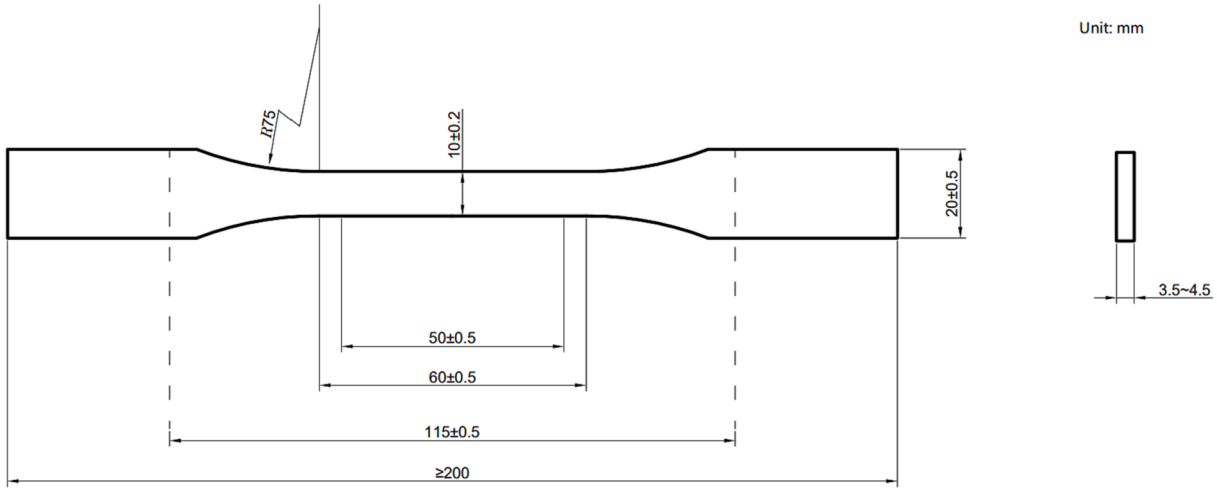

Fig. 1. Tensile test specimen.

Fig. 2. Tensile test of the FRP.

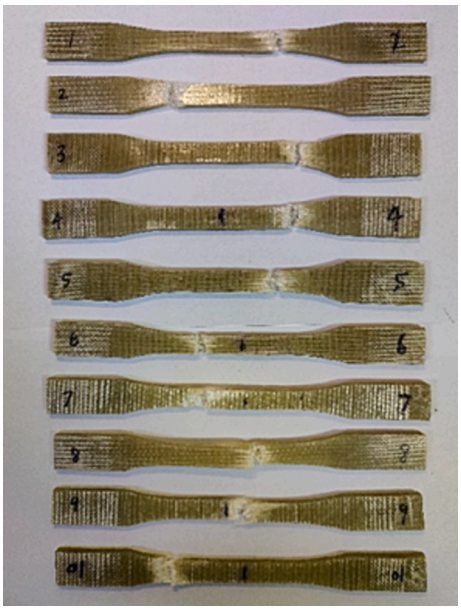

Fig. 3. Damaged specimens after the tensile test.

cover rubber's thickness is 10 mm. The size of the top and bottom connecting plate is 400 × 400 × 15 mm, and the total height of the isolator is 143 mm. The cross-section of the isolator is shown in Fig. 7, and the plan of the isolator is shown in Fig. 8. The first shape factor of the isolator is calculated as S_1.

$$S_1 = \frac{ab}{2(a+b)t_{r1}} = \frac{240 \times 240}{2 \times (240+240) \times 4} = 15 \quad (1)$$

where, a, b and t_{r1} are the length, width and thickness of one FRP plate.

The second shape factor of the isolator is calculated as S_2.

$$S_2 = \frac{b}{t_r} = \frac{240}{48} = 5 \quad (2)$$

where, t_r is the total thickness of the FRP plates in the isolator.

4. Mechanical performance tests of the FRP seismic isolator

4.1. Design of experiments

The vertical and horizontal mechanical performance tests of the FRP seismic isolator use the YJW-20000 model microcomputer control electro-hydraulic servo shear testing machine. It has a maximum loading capacity of 20,000 kN and a maximum displacement capacity of 1000 mm in the vertical direction. It also has a maximum loading capacity of 3000 kN and a maximum displacement capacity of ± 500 mm in the horizontal direction. Accuracy level is first grade. The test force range of the YJW-20000 testing machine is 0.4 %~100 % maximum loading capacity. The accuracy in the force measurement is 1 % of the maximum loading capacity. The accuracy in the displacement measurement is 0.5 % of the maximum displacement capacity.

First, the basic mechanical performance of the FRP seismic isolator is studied through the basic vertical compression performance test and the basic horizontal shear performance test, as shown in Figs. 9-18, respectively. The basic vertical compressive performance test is conducted under the vertical stress of (1 ± 30 %) P_0.P_0 is the vertical design

Table 1
Tensile properties of the FRP.

Specimen No.	Specimen width b (mm)	Specimen thickness a (mm)	Elasticity modulus E ($\times 10^4$ MPa)	Poisson's ratio ν	Tensile strength Rm (MPa)	Elongation at break ε_{t1}(%)	Elongation at maximum load ε_{t2} (%)
1	12.00	4.92	1.7314	0.142	320	3.76	3.76
2	12.16	5.00	1.5023	0.113	225	2.86	2.86
3	10.80	4.52	1.7585	0.138	320	3.80	3.80
4	10.50	4.50	1.9122	0.139	370	3.14	3.14
5	11.58	4.50	1.9156	0.120	345	3.06	3.06
6	11.22	4.40	1.9459	0.139	355	3.57	3.50
7	12.10	4.62	1.7242	0.099	315	3.42	3.42
Average	11.48	4.64	1.7843	0.127	321	3.37	3.37
Dispersion coefficient	0.0575	0.0493	0.0875	0.1309	0.1469	0.1075	0.1075

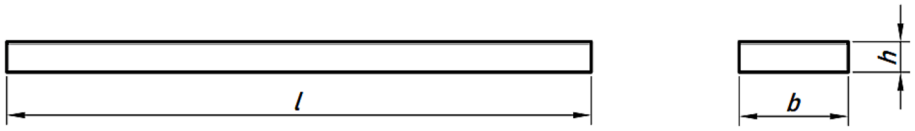

Fig. 4. Bending test specimen.

Fig. 5. Bending test of the FRP.

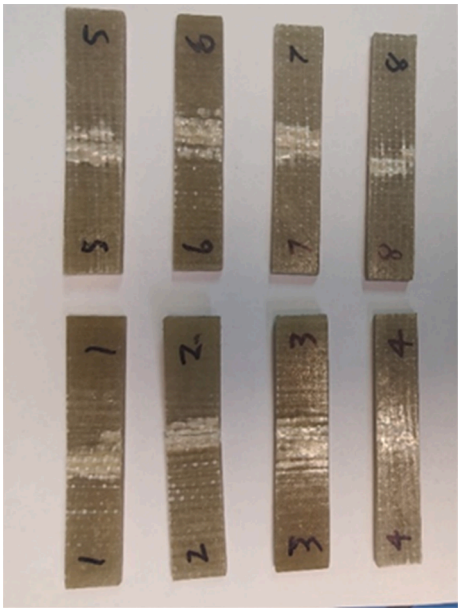

Fig. 6. Damaged specimens after the bending tests.

stress of 5 MPa. Set P_1 as 0.7 times P_0, and set P_2 as 1.3 times P_0. In the basic vertical performance test, the vertical compressive stress is applied in the loading sequence of 0-P_0-P_2-P_0-P_1 (first loading), P_1-P_0-P_2-P_0-P_1 (second loading), and P_1-P_0-P_2-P_0-P_1 (third loading). Three cycles of loading were performed and take third hysteresis loop of the test curve to calculate vertical stiffness, as can be shown in Fig. 19. The basic horizontal shear performance test is investigated by applying vertical stress of 5 MPa and shear deformation up to 100 %γ, where γ is the shear deformation. The basic horizontal shear performance test takes a three-cycle sine wave horizontal force with a loading frequency of 0.05 Hz.

Furthermore, study the shear strain correlation, vertical pressure correlation, and ultimate properties of the FRP seismic isolators. A series of mechanical performance tests were conducted on the FRP isolators as shown in Table 3.

In order to investigate the correlation between the horizontal stiffness and shear strain of the FRP seismic isolator, the FRP seismic isolator is loaded to different shear strain levels under the same vertical compressive stress. The maximum shear strain is loaded to ± 100 %,

Table 2
Bending properties of the FRP.

Specimen No.	Specimen width b (mm)	Specimen thickness a (mm)	Span L_s (mm)	Bending modulus E_f ($\times 10^4$ MPa)	Bending strength f_M (MPa)
1	16.480	5.000	64	5.43	325.00
2	17.660	4.700	64	6.65	380.00
3	15.200	5.000	64	5.79	380.00
4	17.000	5.100	64	5.26	370.00
5	15.900	4.800	64	5.76	370.00
6	16.480	4.520	64	5.93	365.00
7	15.800	4.720	64	6.39	450.00
Average	16.360	4.834	64	5.89	377.14
Dispersion coefficient	0.050	0.043	0	0.084	0.099

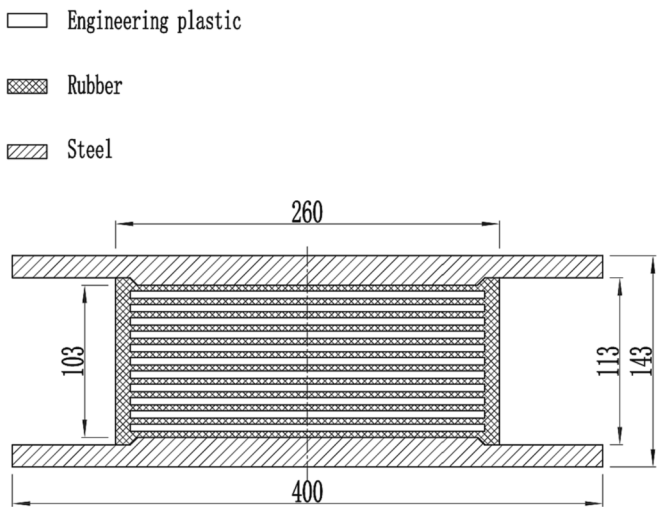

Fig. 7. Cross-section of the FRP seismic isolator.

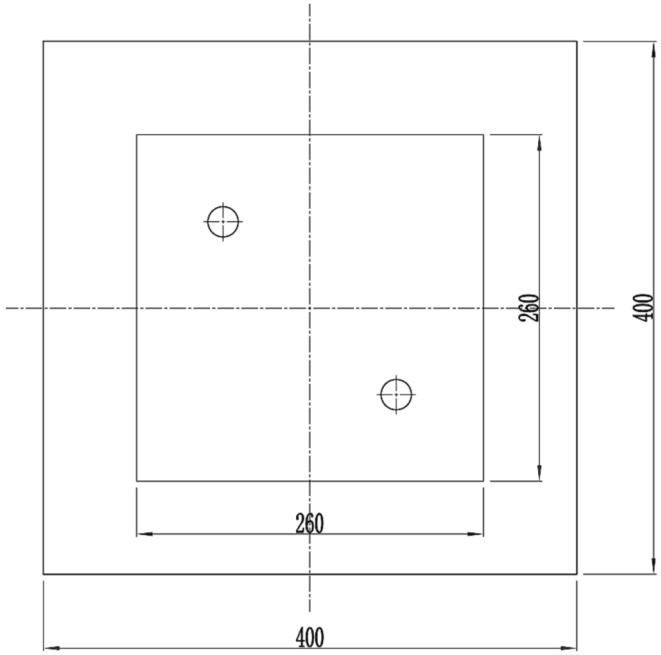

Fig. 8. Plan of the FRP seismic isolator.

±200 %, ±250 %, ±300 %, respectively, and vertical compressive stress is 5 MPa and 10 MPa, respectively.

In order to investigate the correlation between the horizontal stiffness and vertical pressure of the FRP seismic isolator, the FRP seismic isolator is loaded to the same shear strain level under the different vertical compressive stresses. The maximum shear strain is loaded to ± 100 % and ± 200 %, respectively, and vertical compressive stress is 5 MPa, 10 MPa and 15 MPa, respectively.

In order to investigate the correlation between the horizontal stiffness of the FRP seismic isolator and loading frequency, the FRP seismic isolator is subjected to loading frequencies of 0.01 Hz and 0.05 Hz under 5 MPa compressive stress and 100 % shear strain.

In order to test the ultimate vertical capacity of the FRP seismic isolator, the ultimate compressive strength test of the isolator is carried out. Continuously apply vertical compressive stress to the isolator until the isolator is destroyed. In order to investigate the ultimate shear properties of the FRP seismic isolator, the FRP seismic isolator produces

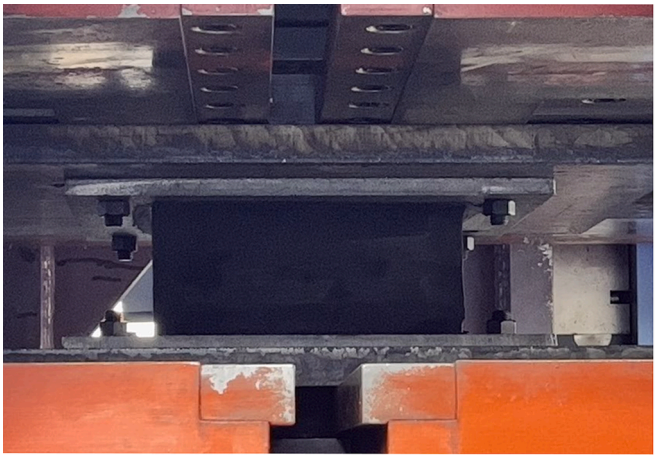

Fig. 9. Vertical compression test (5 MPa).

Fig. 10. Vertical compression test (10 MPa).

Fig. 11. Horizontal shear test (5 MPa-100 %γ).

up to 300 % shear strain under the vertical compressive stress of 5 MPa and 10 MPa.

4.2. *The basic mechanical performance of the FRP seismic isolator*

The vertical compression stiffness is calculated using the third hysteresis loop of the vertical force–displacement curve under 5 MPa, as

Fig. 12. Horizontal shear test (10 MPa-100 %γ).

Fig. 13. Horizontal shear test (5 MPa-200 %γ).

Fig. 14. Horizontal shear test (10 MPa-200 %γ).

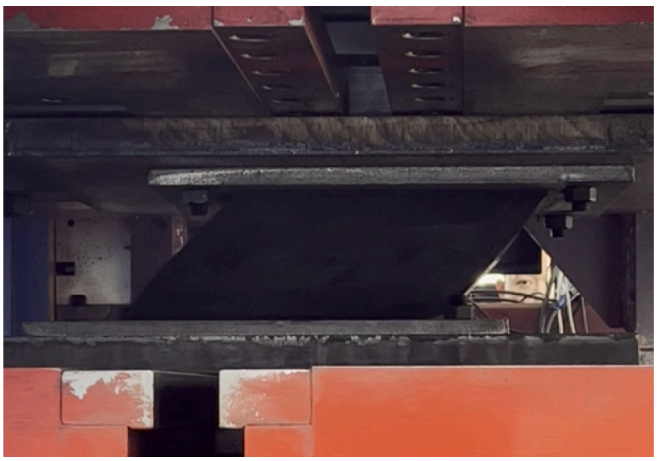

Fig. 15. Horizontal shear test (5 MPa-250 %γ).

Fig. 16. Horizontal shear test (10 MPa-250 %γ).

Fig. 17. Horizontal shear test (5 MPa-300 %γ).

shown in Fig. 19. the horizontal equivalent stiffness is calculated using the third hysteresis loop of the horizontal force–displacement curve under 5 MPa-100 %γ, as shown in Fig. 20. The vertical compression stiffness and horizontal equivalent stiffness are 394.3 kN/mm and 0.70 kN/mm, respectively. The equivalent vertical stiffness can be calculated according to Eq. (3). The equivalent horizontal stiffness can be calculated according to Eq. (4). The equivalent damping ratio can be calculated according to Eq. (5).

$$K_V = \frac{P_2 - P_1}{Y_2 - Y_1} \tag{3}$$

where, K_v is the vertical equivalent stiffness; Y_1 is the displacement corresponding to P_1; Y_2 is the displacement corresponding to P_2.

Fig. 18. Horizontal shear test (10 MPa-300 %γ).

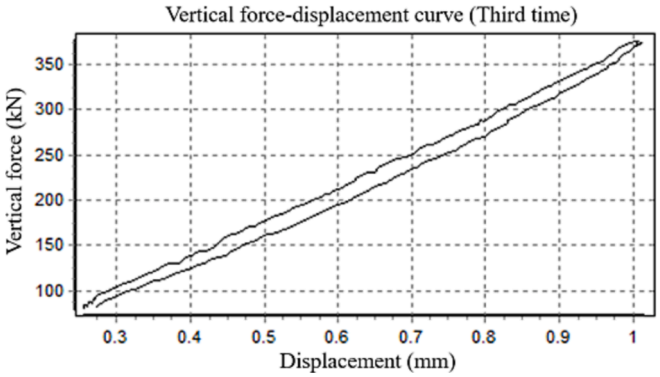

Fig. 19. Vertical force–displacement curve under 5 MPa.

Table 3
The mechanical performance tests of FRP seismic isolators.

Test items	Test conditions	
	Vertical compressive stress (MPa)	Shear strain
The basic vertical compressive performance test	5	0 %
The basic horizontal shear performance test	5	100 %
The shear strain correlation tests	5, 10	100 %, 200 %, 250 %, 300 %
The vertical pressure correlation tests	5, 10, 15	100 %, 200 %
The ultimate vertical properties test	Ultimate compressive stress	0 %
The ultimate shear properties test	10	300 %

$$K_h = \frac{Q_1 - Q_2}{X_1 - X_2} \tag{4}$$

where, K_h is the horizontal equivalent stiffness; Q_1 is the maximum shear force; Q_2 is the minimum shear force; X_1 is the maximum displacement, $X_1 = t_r\gamma$; X_2 is the minimum displacement, $X_2 = t_r(-\gamma)$.

$$h_{eq} = \frac{2\Delta W}{\pi K_h (X_1 - X_2)^2} \tag{5}$$

where, h_{eq} is the equivalent damping ratio; ΔW is the envelope area of the hysteresis curve.

The theoretical vertical stiffness of the steel plate bearing can be calculated according to Eq. (6) [25]. The theoretical horizontal stiffness of the steel plate bearing can be calculated according to Eq. (9).

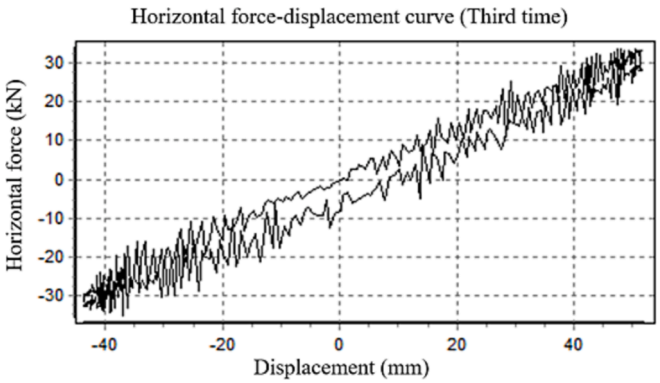

Fig. 20. Horizontal force–displacement curve under 5 MPa-100 %γ.

$$K_V = E_c \frac{A}{t_r} \tag{6}$$

$$E_c = \frac{384}{\pi^4} G S_1^2 (1+\rho^2) \sum_{m=odd}^{\infty} \frac{1}{m^4 \xi_m^2} \left(1 - \frac{2\rho}{m\pi\xi_m} \tanh\left(\frac{m\pi\xi_m}{2\rho}\right)\right) \tag{7}$$

$$\xi_m = \sqrt{1 + \frac{48 G S_1^2 (1+\rho)^2}{K(m\pi)^2}} \tag{8}$$

$$K_h = G \frac{A}{t_r} \tag{9}$$

where, A is the bearing plane area; E_c is the compression modulus; ρ is the aspect ratio of the support plane, $\rho = a/b$; K is the bulk modulus of rubber: G is the shear modulus of rubber;

Suppose our proposed seismic isolation bearing is not made of the FRP plates but of the steel plates. The vertical stiffness of the steel-reinforced seismic isolation bearing calculated by Eq. (6) is 428.4 kN/mm. The horizontal stiffness of the steel-reinforced seismic isolation bearing calculated by Eq. (9) is 0.54 kN/mm. The vertical stiffness test value of the FRP seismic isolation bearing in the paper is 394.3 kN/mm under vertical stress of 5 MPa, which is 8 % less than the horizontal stiffness of the steel-reinforced seismic isolation bearing. The horizontal stiffness test value of the FRP seismic isolation bearing in the paper is 0.7 kN/mm under 5 MPa-100 % shear strain, which is 29 % greater than the horizontal stiffness of the steel-reinforced seismic isolation bearing.

The shear-displacement response of the conventional steel-rubber bearing is linear [26–28] in the 375 % shear strain range. The shear-displacement response of the proposed FRP isolator is also approximately linear, but horizontal stiffness decreases in the range of 100 % ~250 % shear strain and then increases in the range of 250 %~300 % shear strain with the increase of shear strain.

4.3. The correlation of horizontal stiffness and shear strain

The shear strain correlation test results are listed in Table 4. The horizontal stiffness under 5 MPa-200 %, 250 %, and 300 % shear strain is equivalent to 91.43 %, 88.57 %, and 90.00 % of horizontal stiffness under the 5 MPa-100 % shear strain, respectively. The horizontal stiffness under 10 MPa-200 %, 250 %, and 300 % shear strain is equivalent to 95.08 %, 95.08 %, and 100.00 % of horizontal stiffness under the 10 MPa-100 % shear strain, respectively. It can be seen from Table 4 that under vertical stress of 5 MPa, the horizontal stiffness of the bearing decreased from 0.7 kN/mm to 0.62 kN/mm, a decrease of 11.4 %, when the shear strain increased from 100 % to 250 %; and increased from 0.62 kN/mm to 0.63 kN/mm, an increase of 1.6 %, when the shear strain

Table 4
Shear strain correlation test results.

Vertical compressive stress (MPa)	Horizontal shear strain	Horizontal equivalent stiffness (kN/mm)	Equivalent damping ratio
5	100 %	0.70	5.4 %
5	200 %	0.64	5.8 %
5	250 %	0.62	6.0 %
5	300 %	0.63	6.1 %
10	100 %	0.61	7.7 %
10	200 %	0.58	7.6 %
10	250 %	0.58	7.6 %
10	300 %	0.61	7.6 %

increased from 250 % to 300 %. Under vertical stress of 10 MPa, the horizontal stiffness of the bearing decreased from 0.61 kN/mm to 0.58 kN/mm, a decrease of 4.9 %, when the bearing shear strain increased from 100 % to 250 %; and increased from 0.58 kN/mm to 0.61 kN/mm, an increase of 5.2 %, when the bearing shear strain increased from 250 % to 300 %. The change in horizontal stiffness of the bearing was within a stable range of 12 %. Therefore, under the same vertical compressive stress, the horizontal equivalent stiffness of the FRP seismic isolator first decreases and then increases with the increase of shear strain. However, the horizontal equivalent stiffness does not change much in the 100 %-300 % shear strain range.

4.4. The correlation of horizontal stiffness and compressive stress

The compressive stress correlation test results are listed in Table 5. Compared with the shear strain of 5 MPa-100 %γ, the horizontal stiffnesses of 10 MPa-100 %γ and 15 MPa-100 %γ are reduced by 12.86 % and 30.00 %, respectively. Compared with the shear strain of 5 MPa-200 %γ, the horizontal stiffnesses of 10 MPa-200 %γ and 15 MPa-200 %γ are reduced by 9.38 % and 20.31 %, respectively. The horizontal stiffness under 10 MPa is reduced by about 10 % which is an acceptable range, and the horizontal stiffness decreases significantly under 15 MPa, with a decrease of 20–30 %.

4.5. The correlation of horizontal stiffness and loading frequency

The loading frequency correlation test results are listed in Table 6. Under the 5 MPa-100 %γ, with the horizontal force loading frequency increased from 0.01 Hz to 0.05 Hz, the horizontal equivalent stiffness of the FRP seismic isolator increased from 0.66 kN/mm to 0.70 kN/mm, which increases only 6.1 %. It can be seen from Table 6 that the horizontal stiffness of seismic isolation bearing is not sensitive to the loading frequency.

4.6. The ultimate properties of the FRP seismic isolator

The ultimate compressive stress-time curve is shown in Fig. 21. It can be seen that the ultimate compressive stress of the FRP seismic isolator is 36 MPa. The 1/3 ultimate compressive stress, namely 12 MPa, can be taken as the maximum allowable vertical compressive stress of the FRP

Table 5
Compressive stress correlation test results.

Vertical compressive stress (MPa)	Horizontal shear strain	Horizontal equivalent stiffness (kN/mm)	Equivalent damping ratio
5	100 %	0.70	5.4 %
10	100 %	0.61	7.7 %
15	100 %	0.49	10.5 %
5	200 %	0.64	5.8 %
10	200 %	0.58	7.6 %
15	200 %	0.51	10.4 %

Table 6
Loading frequency correlation test results.

Vertical compressive stress (MPa)	Horizontal shear strain	Loading frequency (Hz)	Horizontal equivalent stiffness (kN/mm)	Equivalent damping ratio
5	100 %	0.01	0.66	5.5 %
5	100 %	0.05	0.70	5.4 %

seismic isolator. The horizontal stiffness under 10 MPa-100 %, 200 %, 250 %, and 300 % shear strain is equivalent to 87.14 %, 82.86 %, 82.86 %, and 87.14 % of horizontal stiffness under the 5 MPa-100 % shear strain, respectively. It is judged that the horizontal stiffness of the FRP seismic isolator does not decrease significantly under 10 MPa vertical compressive stress. Therefore, the FRP seismic isolator's maximum allowable vertical compressive stress is defined as 10 MPa to ensure that the isolator remains safe and stable in regular use.

The horizontal force–displacement curves under 5 MPa-300 %γ and 10 MPa-300 %γ have no obvious buckling, as shown in Fig. 22, and the horizontal equivalent stiffnesses of 5 MPa-300 %γ and 10 MPa-300 %γ are shown in Table 4.

From Fig. 22 and Table 4, it can be seen that: Compared with the horizontal stiffness of 5 MPa-100 %γ, the horizontal stiffness of 5 MPa-300 %γ is reduced by 12.86 %, and compared with the horizontal stiffness of 10 MPa-100 %γ, the horizontal stiffness of 10 MPa-300 %γ is reduced by 30.00 %. So that the ultimate shear strain can reach 300 %.

5. Numerical analysis of the FRP seismic isolator

5.1. Finite element model

Finite element modelling of the FRP seismic isolator was carried out with Abaqus software [29]. The FRP plate is simulated using C3D8 elements, and its elasticity modulus is 17.84 GPa. The rubber is simulated using the C3D8H hybrid elements. C3D8H element is intended primarily for use with incompressible and almost incompressible material behavior. Rubber is typically an incompressible material, so it is appropriate to use the C3D8H element to simulate rubber behavior. The material model of the rubber uses the Ogden (N = 3) model, which is stable within 700 % strain. The Ogden intrinsic model used for rubber materials is a molecular grid model based on rubber elasticity. The strain energy density function of the Ogden model is expressed by the principal stretches as variables, as follows:

$$U = \sum_{i=1}^{N} \frac{2\mu_i}{\alpha_i^2}\left(\overline{\lambda}_1^{\alpha_i} + \overline{\lambda}_2^{\alpha_i} + \overline{\lambda}_3^{\alpha_i} - 3\right) + \sum_{i=1}^{N} \frac{1}{D_i}(J-1)^{2i} \tag{10}$$

Where $\overline{\lambda}_i$ are deviatoric principal stretches, $\overline{\lambda}_i = J^{-1/3}\lambda_i$ (i = 1,2,3), λ_i, λ_2 and λ_3 are the principal stretches; J is the volume ratio of rubber before and after deformation; D_i is a parameter that measures the degree of compressibility of rubber, if D_i is 0, the material is incompressible; μ_i and α_i are material parameters, which can be obtained by experimental fitting.

The initial shear modulus μ_0 and initial bulk modulus K_0 are given by:

$$\mu_0 = \sum_{i=1}^{N} \mu_i,\ K_0 = \frac{2}{D_1} \tag{11}$$

The rubber's material parameters are as follows: μ_1=0.63388 MPa, α_1=0.102, μ_2=5.07104 × 10^{-7} MPa, α_2=2.006, μ_3=0.038584 MPa, α_3=4.114, K_0=2430 MPa. Since there was no mutual peeling between the layers of materials during the isolator's mechanical performance test, use the 'Partition cell' command to split the entire model so that two faces of adjacent layers in contact with each other become one face to ensure a reliable connection between adjacent layers. This method

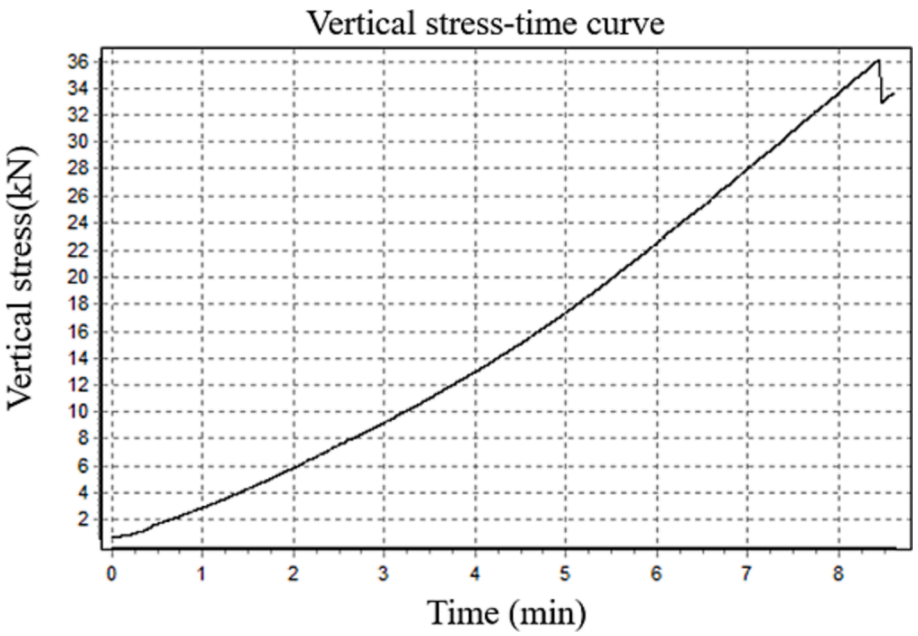

Fig. 21. Ultimate compressive stress-time curve.

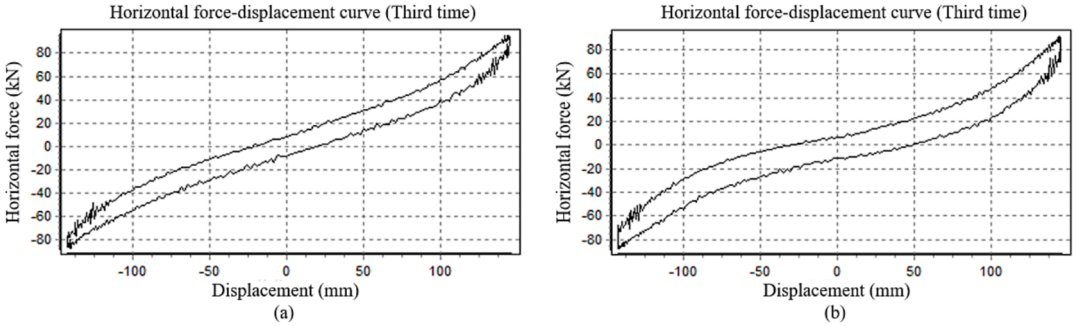

Fig. 22. Horizontal force–displacement curves under 300 %γ (a) 5 MPa, (b) 10 MPa.

reduces the number of nodes generated after mesh generation and avoids the contact nonlinearity problem arising from 'tie' constraint connections between different material layers.

To accurately simulate the deformation of the inner rubber layer, the rubber layer is divided into four units vertically and 40 units horizontally. The FRP plate is divided into two units vertically and 40 units horizontally; the steel plate is divided into three units vertically and 66 units horizontally. The isolator's finite element model is shown in Fig. 23.

5.2. *Verification of the finite element model*

The finite element analysis of the FRP seismic isolator under 5 MPa-100 %, 200 %, 250 %, and 300 % shear strain is carried out, as shown in

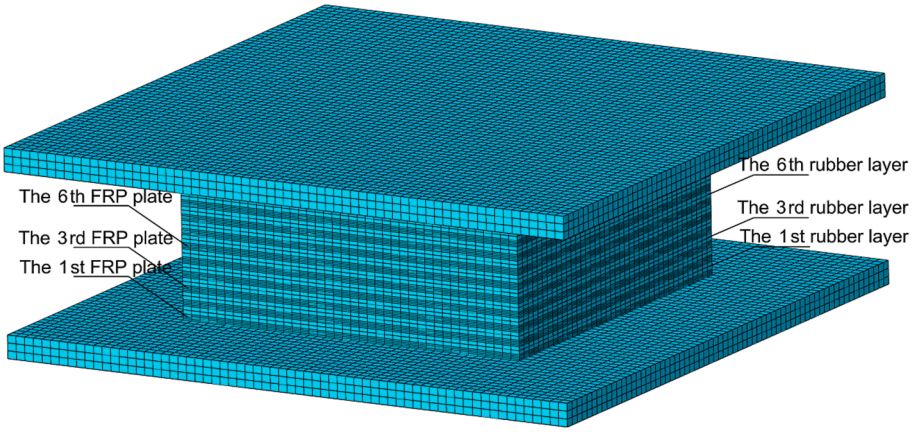

Fig. 23. Three-dimensional model of isolator.

Table 7
Comparison of simulated and tested values of the horizontal equivalent stiffness.

Test conditions	Horizontal equivalent stiffness (kN/mm)		The simulated value/The tested value
	The tested value	The simulated value	
5 MPa-100 %	0.70	0.70	1
5 MPa-200 %	0.64	0.61	0.953
5 MPa-250 %	0.62	0.60	0.968
5 MPa-300 %	0.63	0.61	0.968

Table 7. The maximum error between the simulated and experimental values of the horizontal equivalent stiffness of the FRP seismic isolator is only 4.7 %, so the simulation result of the FRP seismic isolator has high reliability. The horizontal force–displacement curves of FEM under 5 MPa-100 %γ and 300 %γ are shown in Fig. 24 and Fig. 25, respectively. The hysteresis curve of the isolator is approximately a straight line.

5.3. Horizontal stress analysis of the FRP seismic isolator

The stresses of the first, third, and sixth layers of the FRP plate are extracted to study the relationship between the distribution of horizontal normal stress of FRP plates and the shear strain of the FRP seismic isolator. The distribution of horizontal normal stress along the length of the FRP plate is shown in Fig. 26.

Fig. 26 shows that the peak horizontal normal stress of the FRP plate gradually shifts from the center to the ends of the FRP seismic isolator as the shear strain increases. With the increase of shear strain, due to the decrease of the effective loaded area of the FRP seismic isolator, the peak horizontal normal tensile stress of the FRP plate increases. The maximum horizontal stress appears in the middle of the first layer plate under the 5 MPa-100 % shear strain and moves to the right along the plate length as the shear strain increases. As seen in Fig. 26, from 100 % to 300 % shear strain, the peak horizontal stress of the sixth layer plate increased from 6.49 MPa to 10.84 MPa, which increased by 67.03 %. The peak horizontal stress of the third layer plate increased from 6.58 MPa to 12.21 MPa, which increased by 85.56 %. The peak horizontal stress of the first layer plate increased from 6.58 MPa to 12.90 MPa, which increased by 96.04 %. The increase of peak horizontal tensile stress of the first plate layer is more significant than that of other plate layers.

5.4. Vertical stress analysis of the FRP seismic isolator

The vertical normal stress between the first, third and sixth rubber layers under the compressive stress of 5 MPa and shear strain of 100 %, 200 %, 250 %, and 300 % is shown in Fig. 27. Fig. 27 shows that the rubber layer's peak vertical compressive stress increases with the growth of shear deformation, and its position moves with the direction

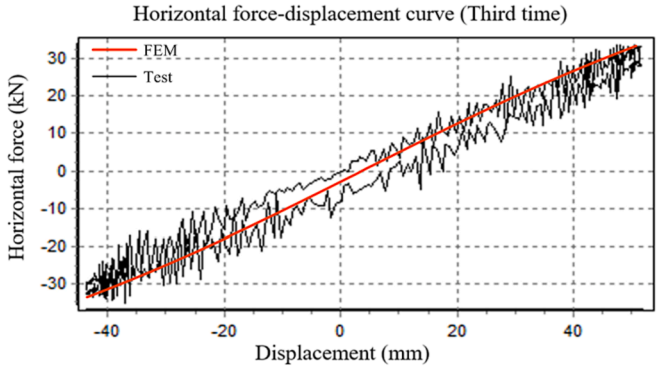

Fig. 24. Horizontal force–displacement curve of FEM under 5 MPa-100 %γ.

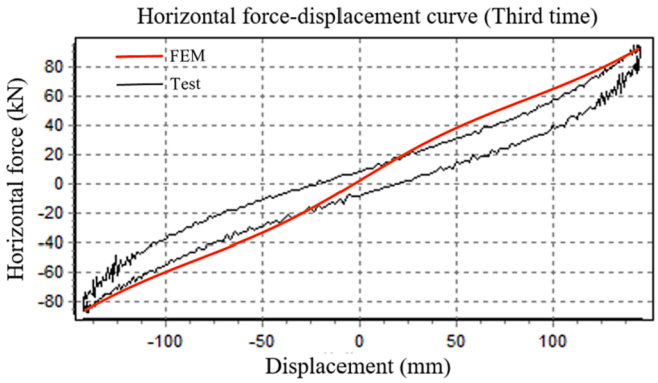

Fig. 25. Horizontal force–displacement curve of FEM under 5 MPa-300 %γ.

of shear deformation. With the increase of shear strain, the cross-section of the FRP plates and rubber layers changes from rectangular to parallelogram. The rubber layer in the diagonal acute angle regions of the parallelogram is in the vertical tension state. Because the isolator's vertical load position changes as the isolator's shear strain increases, the horizontal shear force and the vertical stress cause the P-Δ effects, resulting in large vertical and horizontal normal tensile stress in the acute angle regions at both ends of the isolator. And with the growth of the isolator deformation, the scope of the rubber layer under biaxial tension gradually expands.

5.5. Interfacial shear stress analysis of the FRP seismic isolator

The interfacial shear stress between the first, third and sixth rubber layer and the FRP plate under the compressive stress of 5 MPa and shear strain of 100 %, 200 %, 250 %, and 300 % is shown in Fig. 28. Fig. 28 shows that when the shear strains reach 100 %, 200 %, 250 %, and 300 %, the peak shear stresses are 0.81 MPa, 1.37 MPa, 1.75 MPa, and 2.14 MPa, respectively, which are 0.162, 0.274, 0.35, and 0.428 times of the vertical pressure, respectively. Under minor shear strain, the interfacial shear stresses at different locations are relatively similar. With the growth of shear deformation, the peak interfacial shear stress of the sixth rubber layer and FRP plate gradually exceeds that of the other layers and becomes the new peak point position.

6. Numerical simulation study of the effect of dimensional change of seismic isolators

6.1. Horizontal stress analysis of the rectangular FRP seismic isolator

The rectangular isolator with a plane size of 480 × 240 mm is designed. The rectangular isolator's vertical and horizontal mechanical properties are analyzed and compared with the square isolator's. The contours of horizontal normal stresses of the sixth FRP plate of square isolator and rectangular isolator under the vertical stress of 5 MPa are compared in Fig. 29 and Fig. 30.

Fig. 29 and Fig. 30 show that the peak horizontal normal stresses in the FRP seismic isolator occur at the center of the plate, and the peak horizontal normal stresses in the rectangular and square isolator are 6.68 MPa and 5.70 MPa, respectively.

The contours of horizontal stresses of the square isolator and rectangular isolator under the 5 MPa compressive stress and 300 % shear strain are compared in Fig. 31. It can be seen from Fig. 31 that both of the square and rectangular isolators' peak horizontal normal stresses are tensile stress, which appears at the end of the first FRP plate. And the peak horizontal tensile stress of the rectangular isolator is 2.05 times that of the square isolator. The horizontal normal stresses of both isolators are concentrated in the obtuse angle regions of the bearing section. The horizontal stress in the remaining areas is small. The horizontal

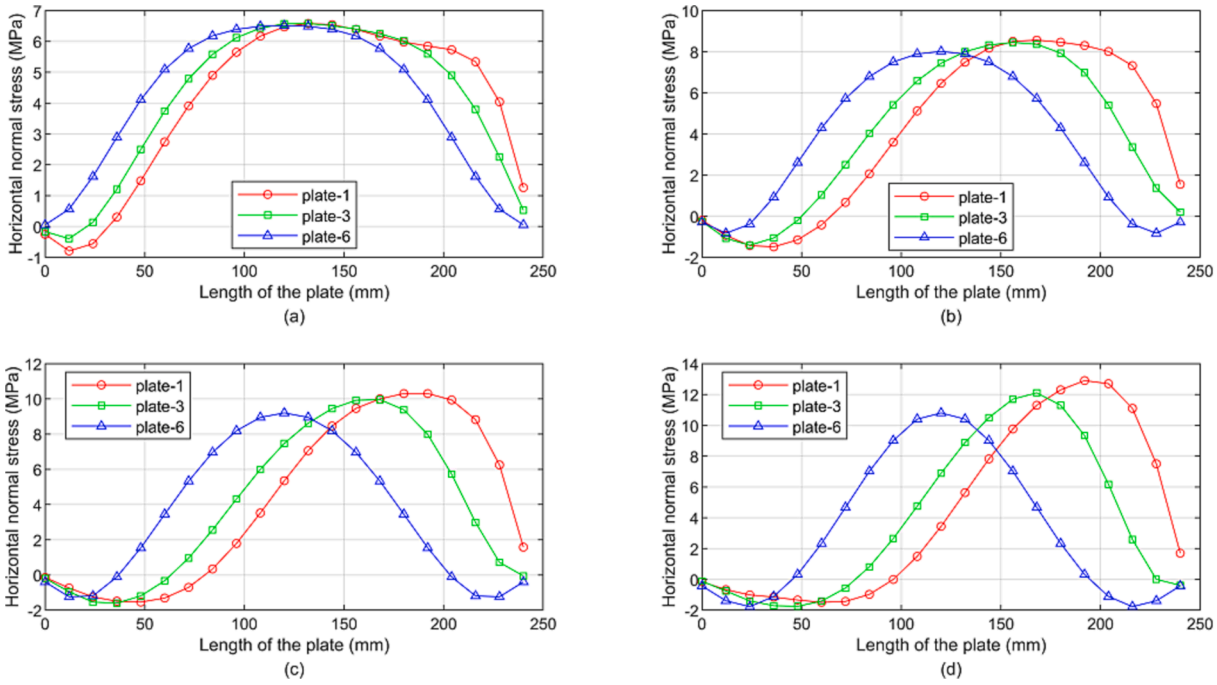

Fig. 26. Distributions of horizontal normal stresses under 5 MPa-(a) 100 %γ, (b) 200 %γ, (c) 250 %γ, and (d) 300 %γ.

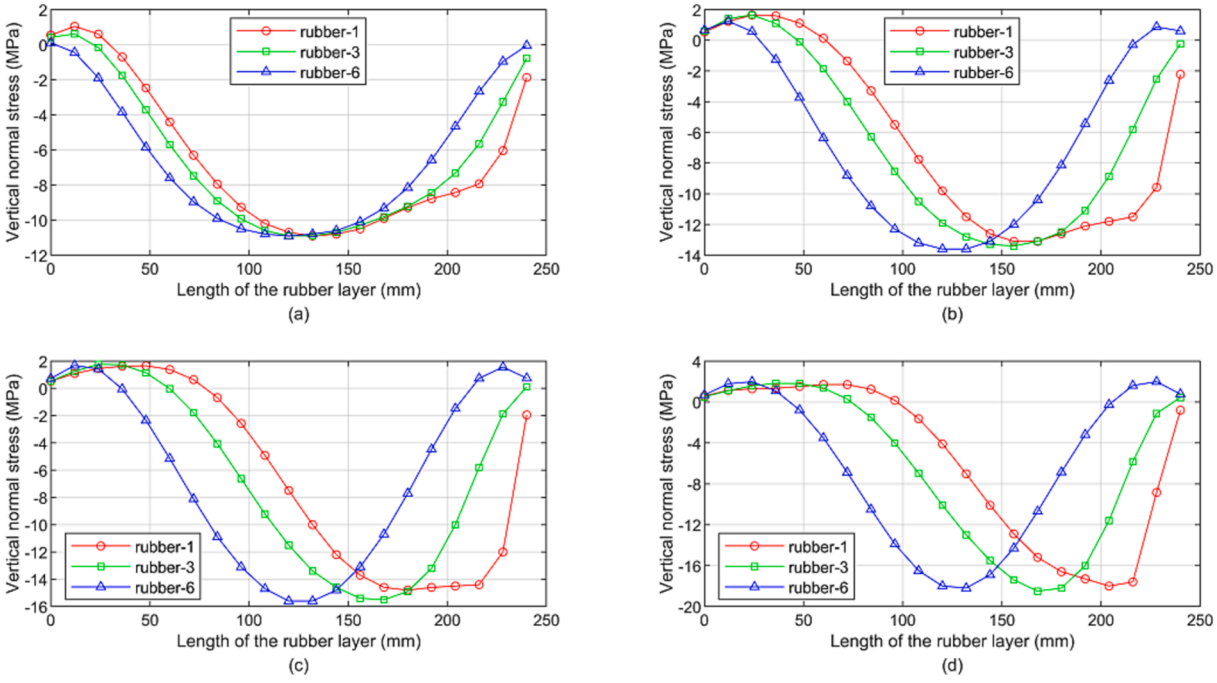

Fig. 27. Distributions of vertical normal stresses under 5 MPa-(a) 100 %γ, (b) 200 %γ, (c) 250 %γ, and (d) 300 %γ.

normal stress distributions are similar for square and rectangular isolators.

The horizontal stiffness of the rectangular isolator calculated by Eq. (9) is 1.08 kN/mm. The horizontal stiffness of the numerical simulation is 1.22 kN/mm under 5 MPa-300 % shear strain, which is 13 % greater than the theoretical value of horizontal stiffness. The simulated stiffnesses are in good agreement with the theoretical values.

The horizontal equivalent stiffnesses of the rectangular isolator under the vertical compressive stress of 5 MPa and shear strain of 100 %, 200 %, 250 %, 300 % are simulated, as shown in Table 8. Table 8 shows that the horizontal stiffnesses along the short axis direction of the rectangular isolator are 2.02, 2.01, 2.00, and 2.00 times that of the square isolator under the shear strain of 100 %, 200 %, 250 %, and 300 %, respectively. The horizontal stiffnesses along the long axis direction of the rectangular isolator are 2.06, 2.04, 2.03, and 2.03 times that of the square isolator under the shear strain of 100 %, 200 %, 250 %, and 300 %, respectively. It can be seen from Table 8 that the difference in horizontal stiffness of rectangular isolator in the long and short axis directions does not exceed 2 %. The horizontal equivalent stiffness of the rectangular isolator does not differ much when shear strain occurs along the short axis direction and the long axis direction of the rectangular isolator. The difference shows that the horizontal stiffness of the isolator

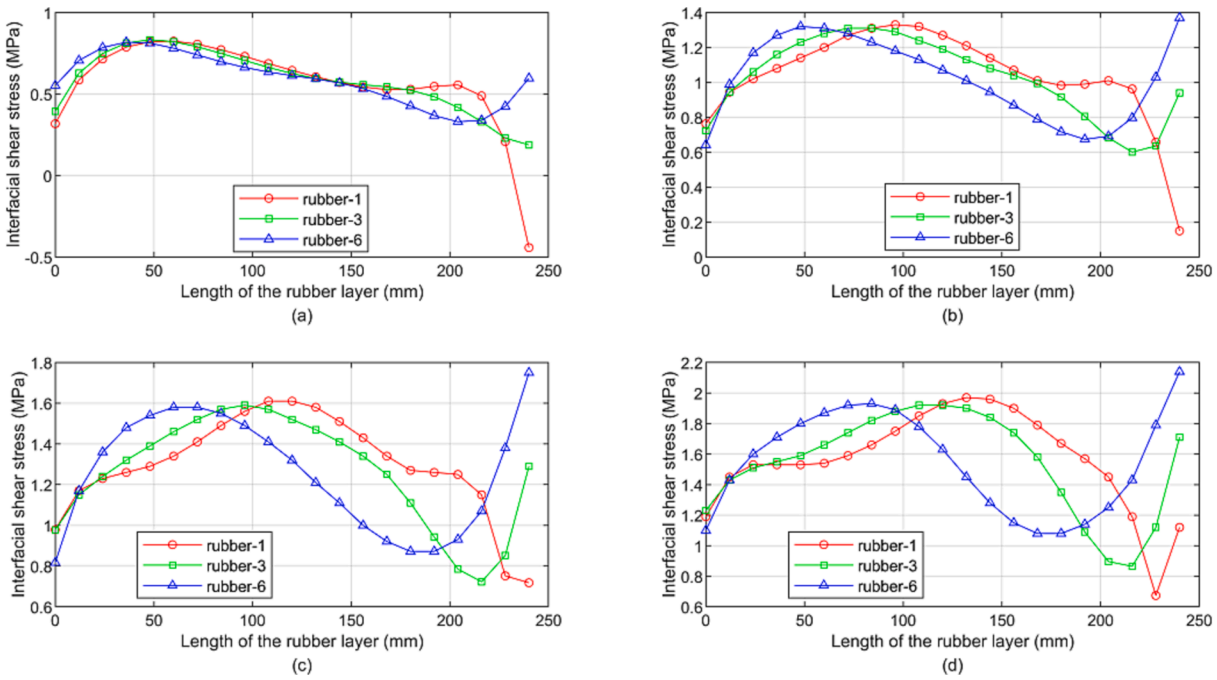

Fig. 28. Distributions of interfacial shear stresses under 5 MPa-(a) 100 %γ, (b) 200 %γ, (c) 250 %γ, and (d) 300 %γ.

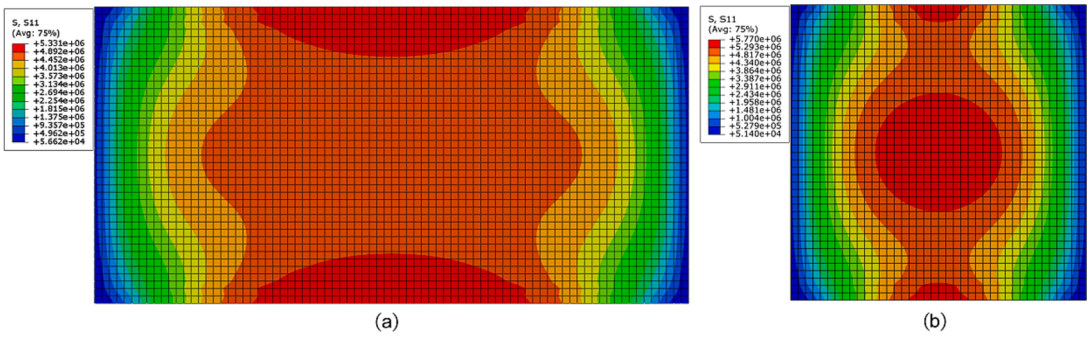

Fig. 29. Contours of horizontal stress in the long-axis direction of the sixth FRP plate (a) rectangular isolator, (b) square isolator.

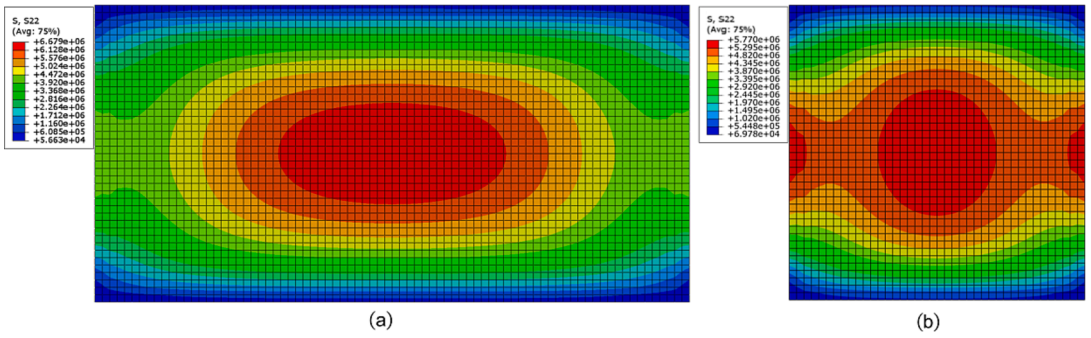

Fig. 30. Contours of horizontal stress in the short-axis direction of the sixth FRP plate (a) rectangular isolator, (b) square isolator.

is not related to the direction of the shear strain.

The maximum horizontal normal stresses of the FRP plate inside rectangular and square isolators are compared in Table 9, which shows that the increase of the isolator plane size decreases the internal unbalance moment of the isolator and weakens the P-Δ effects. When the isolator shear deformation occurs, the FRP plate of the rectangular isolator is subjected to less horizontal normal tensile stress than that of the square isolator, and the greater the shear strain, the more pronounced the decline.

The horizontal stress distributions of the first, third, and sixth FRP plate inside the rectangular isolator under different shear strains along the long axis are shown in Fig. 32. It can be seen from Fig. 26 and Fig. 32 that the rectangular isolator has a core compression zone with broader scope and larger area than square isolators at the same shear deformation level, which results in a lower peak horizontal tensile stress in the FRP plates.

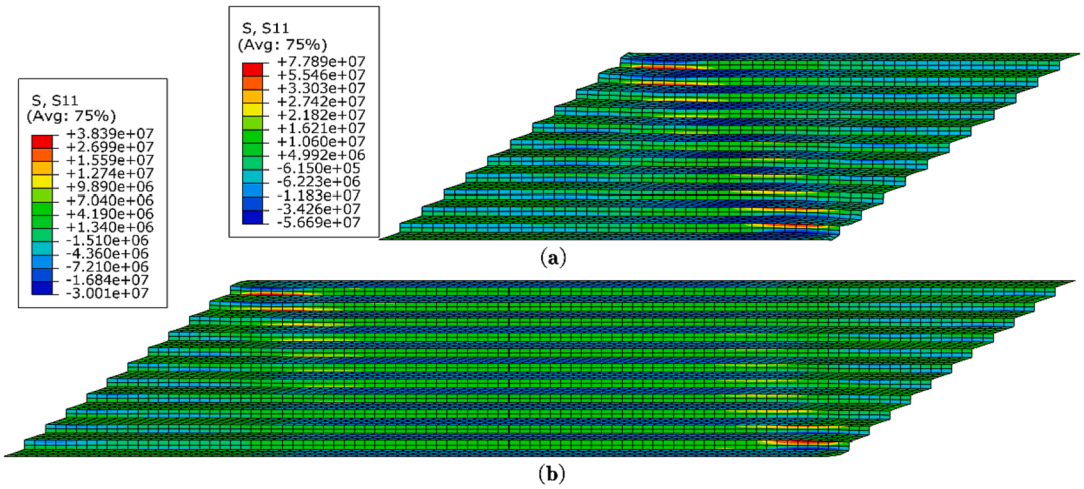

Fig. 31. Contours of horizontal stresses under 5–300 %γ of (a) square isolator and (b) rectangular isolator.

Table 8
The horizontal equivalent stiffness of rectangular isolators.

Boundary condition	Horizontal equivalent stiffness (kN /mm)		$(K_{hl}-K_{hs})/K_{hs}$
	Short axis K_{hs}	Long axis K_{hl}	
5 MPa-100 %	1.414	1.442	1.98 %
5 MPa-200 %	1.226	1.245	1.55 %
5 MPa-250 %	1.197	1.215	1.50 %
5 MPa-300 %	1.217	1.241	1.97 %

Table 9
Maximum horizontal normal stresses of the FRP seismic isolators.

Boundary condition	Maximum horizontal tensile stress of plate (MPa)		Rectangular/Square
	Square	Rectangular	
5 MPa-100 %	6.58	4.91	74.62 %
5 MPa-200 %	8.56	5.60	65.42 %
5 MPa-250 %	10.30	5.92	57.48 %
5 MPa-300 %	12.90	6.30	48.83 %

The peak horizontal tensile stresses in each FRP plate of the rectangular and square bearing both increase with the increase of shear strain. The peak horizontal tensile stress of the square bearing always appears in the first FRP plate. The peak horizontal tensile stress of the rectangular bearing appears in the sixth FRP plate under the 100 % shear strain and in the first FRP plate under the 200 %~300 % shear strain. When the shear strain increased from 100 % to 300 %, the peak horizontal tensile stress of rectangular bearing increased from 4.91 MPa to 6.30 MPa, an increase of 28.31 %, and the peak horizontal tensile stress of square bearing increased from 6.58 MPa to 12.90 MPa, an increase of 96.05 %. The peak horizontal tensile stress of square bearing increased more significantly than that of rectangular bearing with the increase of shear strain.

6.2. *Vertical stress analysis of the rectangular FRP seismic isolator*

The maximum vertical normal stresses of the rubber layer inside rectangular and square isolators are compared in Table 10. The vertical stress distributions of the sixth rubber layer inside rectangular and square isolators are compared in Fig. 33. It can be seen from Table 10 and Fig. 33 that the sixth rubber layers of rectangular and square isolators are subjected to tensile forces at the ends and compressive forces in the middle area. The tensile and compressive areas of the rectangle isolator are larger than those of the square isolator, and the stress distribution of the rectangular isolator is more uniform.

The peak compressive stresses of both the rectangular and square bearing appear in the middle of the sixth rubber plate, and the peak tensile stresses appear at both ends of the sixth rubber layer. It can be seen from Table 10 that the difference between the peak vertical stress in the rectangular and square bearing is the largest at a shear strain of 300 %. Under the 5 MPa-300 % shear strain, the maximum vertical tensile stress of the rectangular isolator is 0.83 times that of the square isolator, and the maximum vertical compressive stress is 0.65 times that of the square isolator. The peak vertical stresses of the rectangular bearing are smaller than those of the square isolator.

From 100 % to 200 %, 250 %, and 300 % shear strain, the peak vertical tensile stresses increased by 629.41 %, 35.48 %, and 17.86 % for the square FRP seismic isolators, and by 625 %, 20.69 %, and 17.14 % for the rectangular FRP seismic isolators, respectively. From 100 % to 200 %, 250 %, and 300 % shear strain, the peak vertical compressive stresses increased by 25.21 %, 43.42 %, and 67.25 % for the square FRP seismic isolators, and by 13.14 %, 19.30 %, and 25.98 % for the rectangular FRP seismic isolators, respectively. The peak vertical tensile and compressive stress of the square isolator increases more significantly than that of the rectangular isolator with the increase of shear strain.

6.3. *Interfacial shear stress analysis of the rectangular FRP seismic isolator*

The maximum interfacial shear stresses of the FRP plate inside rectangular and square isolators are compared in Table 11. The distributions of the interfacial shear stress between the first, third and sixth rubber layers and FRP plates inside the rectangular isolator are shown in Fig. 34.

It can be seen from Table 11, Fig. 28, and Fig. 34 that the peak interfacial shear stress of the FRP seismic isolator is not significantly affected by the isolator plane size. The shear stress at the end of the plate increases gradually with the increase in shear strain, and the end of the plate becomes the location of the peak interfacial shear stress.

7. Analysis of the effect of P/RTR on the horizontal shear performance of the FRP seismic isolator

The stiffness of the FRP seismic isolator depends mainly on the thickness of the FRP plates and internal rubber layers. Therefore, the excessive P/RTR will lead to large horizontal stiffness, thus affecting the seismic isolation effect. In order to investigate the effects of the P/RTR on the isolator's horizontal shear performance, FRP seismic isolators

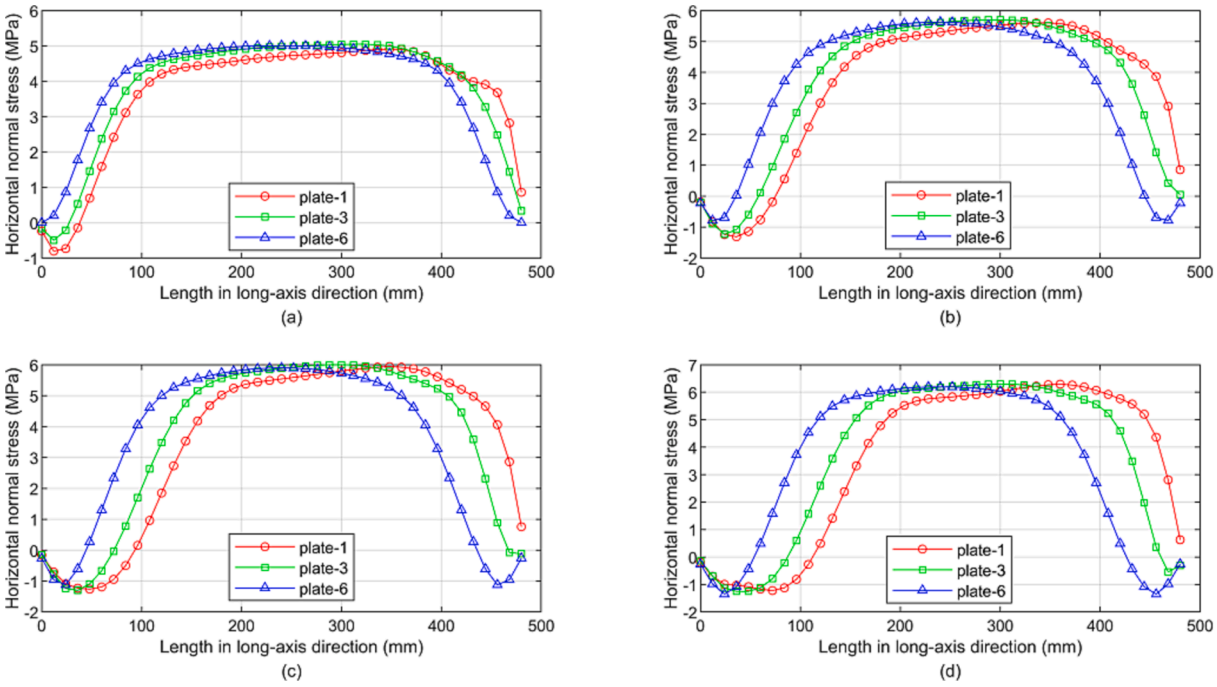

Fig. 32. Distributions of horizontal normal stresses along the long-axis under 5 MPa-(a) 100 %γ, (b) 200 %γ, (c) 250 %γ, and (d) 300 %γ.

Table 10
Maximum vertical normal stresses of the FRP seismic isolators.

Boundary condition	Maximum vertical tensile stress of plate (MPa)		Maximum vertical compressive stress of plate (MPa)	
	Square	Rectangular	Square	Rectangular
5 MPa-100 %	0.17	0.16	10.87	9.43
5 MPa-200 %	1.24	1.16	13.61	10.67
5 MPa-250 %	1.68	1.40	15.59	11.25
5 MPa-300 %	1.98	1.64	18.18	11.88

Table 11
Maximum horizontal normal stresses of the FRP plate.

Boundary condition	Maximum interfacial shear stress of plate (MPa)		Rectangular/Square
	Square	Rectangular	
5 MPa-100 %	0.81	0.77	95.06 %
5 MPa-200 %	1.37	1.36	99.27 %
5 MPa-250 %	1.75	1.68	96.00 %
5 MPa-300 %	2.14	2.02	94.39 %

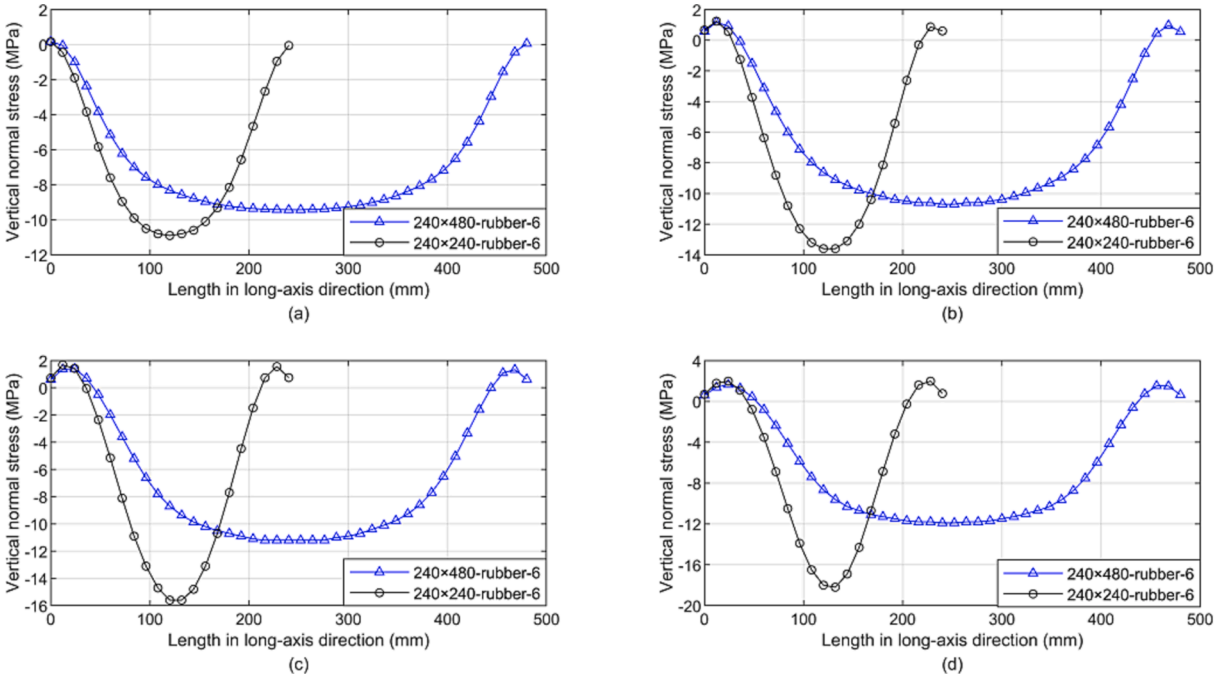

Fig. 33. Distributions of vertical normal stresses inside rectangular and square isolators under 5 MPa-(a) 100 %γ, (b) 200 %γ, (c) 250 %γ, and (d) 300 %γ.

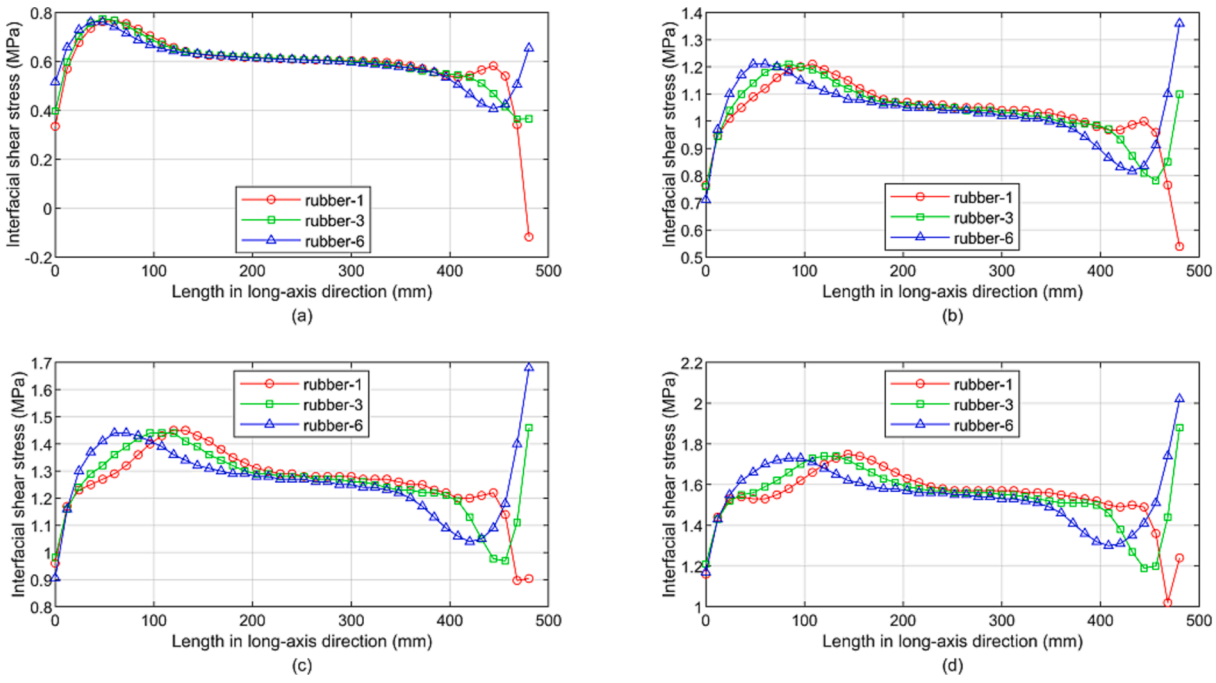

Fig. 34. Distributions of interfacial shear stresses along the long-axis under 5 MPa-(a) 100 %γ, (b) 200 %γ, (c) 250 %γ, and (d) 300 %γ.

with different P/RTR are designed to perform numerical simulation analysis. Parameters of the FRP seismic isolator models are shown in Table 12. In this paper, the P/RTR of the steel plate rubber laminated bearing is referred to, and a suitable range of P/RTR is selected. The P/RTR is between 0.8 and 1.2. The P/RTR selected in this paper can study the effect of the P/RTR on the stress distribution of the bearing.

7.1. Influence of P/RTR on the horizontal stress

The position of peak horizontal tensile stress appears at the first FRP plate, so the horizontal normal stresses of the first FRP plate in the FRP seismic isolators with different P/RTR are extracted, as shown in Fig. 35. It is shown in Fig. 35 that the shape of the horizontal stress distribution is not affected by the P/RTR. The horizontal compressive stress appears at the left end of the first plate layer. The compressive stress increases to peak compressive stress along with the plate's length from left to right then decreases to 0 MPa and gradually becomes horizontal tensile stress. The horizontal tensile stress increases to peak horizontal tensile stress and then decreases from left to right.

The peak horizontal tensile stresses at 5 MPa-100 % shear strain are 6.58 MPa, 8.40 MPa, and 11.16 MPa for the 1.2, 1, and 0.8P/RTR, respectively. The peak horizontal tensile stresses at 5 MPa-200 % shear strain are 8.56 MPa, 10.88 MPa, and 14.75 MPa for the 1.2, 1, and 0.8P/RTR, respectively. The peak horizontal tensile stresses at 5 MPa-300 % shear strain are 12.90 MPa, 15.53 MPa, and 27.22 MPa for the 1.2, 1, and 0.8P/RTR, respectively. Therefore, the increase in the P/RTR reduces the peak horizontal tensile stress in the FRP plates.

7.2. Influence of P/RTR on the vertical stress

From Fig. 27, it can be seen that at 5 MPa-100 % shear strain, the vertical stress of the first rubber layer of the isolator is maximum, so the vertical normal stresses of the first rubber layer are extracted, as shown in Fig. 36. It can be seen from Fig. 36 that the vertical stress distribution of the 1.2P/RTR and the 1P/RTR is almost the same. The reason for this phenomenon is that the rubber thickness is the same resulting in the same shear strain. Thus, the vertical stress distribution of the plate is the same when the rubber layers' thickness are the same. It can be seen from Fig. 36 that the peak vertical normal stress of the 0.8P/RTR is greater than that of the 1.2 and 1P/RTR. The reason for this phenomenon is that the increase in rubber thickness leads to an increase in shear strain and a decrease in the effective loaded area of the isolator. Thus, the vertical stress increases when the rubber layers' thickness increases. The vertical normal stress of the inner rubber layer is affected by the strain of the rubber layer. If the thickness of the rubber layer is constant, the peak vertical normal stress is unchanged. The peak vertical normal stress is increased by increasing the thickness of the rubber layer.

7.3. Influence of P/RTR on the interfacial shear stress

As the peak interfacial shear stress position appears between the sixth FRP plate and rubber layer, the interfacial stress distributions between the sixth FRP plate and rubber layer are extracted, as shown in Fig. 37. It can be seen from Fig. 37 that the peak interfacial shear stress is affected by the strain of the rubber layers. Comparing the 1.2P/RTR and the 1P/RTR, the interfacial stress value of the plate layer is almost the same. It can be concluded that the interfacial stress is the same when the

Table 12
Parameters of FRP seismic isolators with different P/RTR.

NO.	Isolator parameters/mm					
	Length × Width	Thickness of a single FRP plate × Quantity	Thickness of a single rubber sheet × Quantity	Connecting plate thickness	Isolator total high	Thickness ratio
M−1	240 × 240	5 × 11	4 × 12	15	133	1.2
M−2	240 × 240	4 × 11	4 × 12	15	122	1
M−3	240 × 240	4 × 11	5 × 12	15	134	0.8

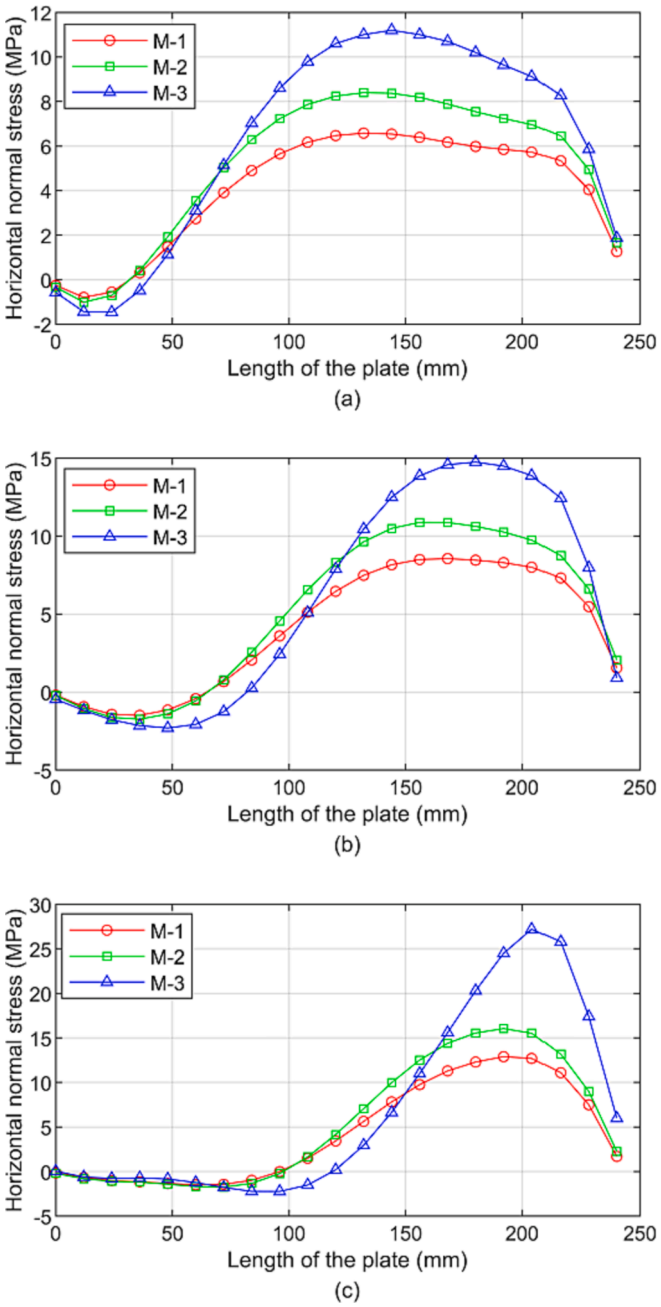

Fig. 35. Distributions of horizontal normal stresses of the first plate layer under 5 MPa-(a) 100 %γ, (b) 200 %γ, and (c) 300 %γ.

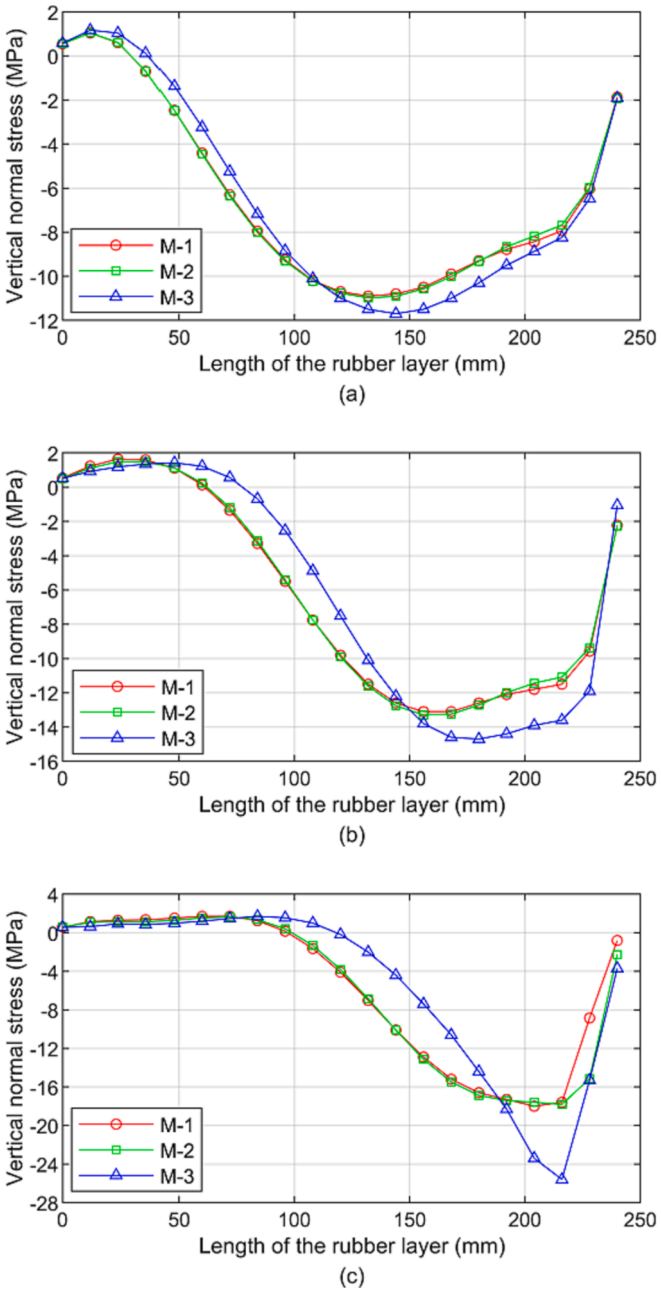

Fig. 36. Distributions of vertical normal stresses of the first rubber layer under 5 MPa-(a) 100 %γ, (b) 200 %γ, and (c) 300 %γ.

thickness of the rubber layer is the same.

The peak interfacial shear stress under the shear strain of 100 % is located at 1/5 of the plate length from the left end of the layer. The peak interfacial shear stresses under the shear strain of 200 % and 300 % are at the right end of the layer. The peak interfacial shear stresses were 0.82 MPa, 1.39 MPa, 2.18 MPa for the 1P/RTR and 0.87 MPa, 1.55 MPa, 1.99 MPa for the 0.8P/RTR under the 5 MPa-100 %, 200 %, 300 % shear strain, respectively. The peak interfacial shear stress is only related to rubber thickness, not to plate thickness. The peak interfacial shear stresses increase with increasing of rubber thickness under the shear strains of 100 % and 200 %, and decrease under the shear strain of 300 %.

8. Conclusions

This paper developed a new type of low-cost seismic isolator, which replaced the steel plate in the traditional rubber seismic isolator with FRP plates. The FRP plate used as stiffening plate is made of vinyl resin and alkali-free cloth. The FRP seismic isolator is designed with upper and lower sealing plates to increase its stability, and the FRP plate is processed by brushing and other processes to increase the adhesion between the FRP plate and rubber. Firstly, the mechanical performances of FRP plates were tested by tensile and bending tests of the FRP plates. The tests showed that both of the tensile and bending strengths of the FRP plate are greater than 170 MPa, which could be used as the stiffening plate in the rubber seismic isolator.

Secondly, The mechanical performances of the FRP seismic isolator were tested by the vertical compressive performance test, horizontal shear performance test, ultimate performance test, shear strain

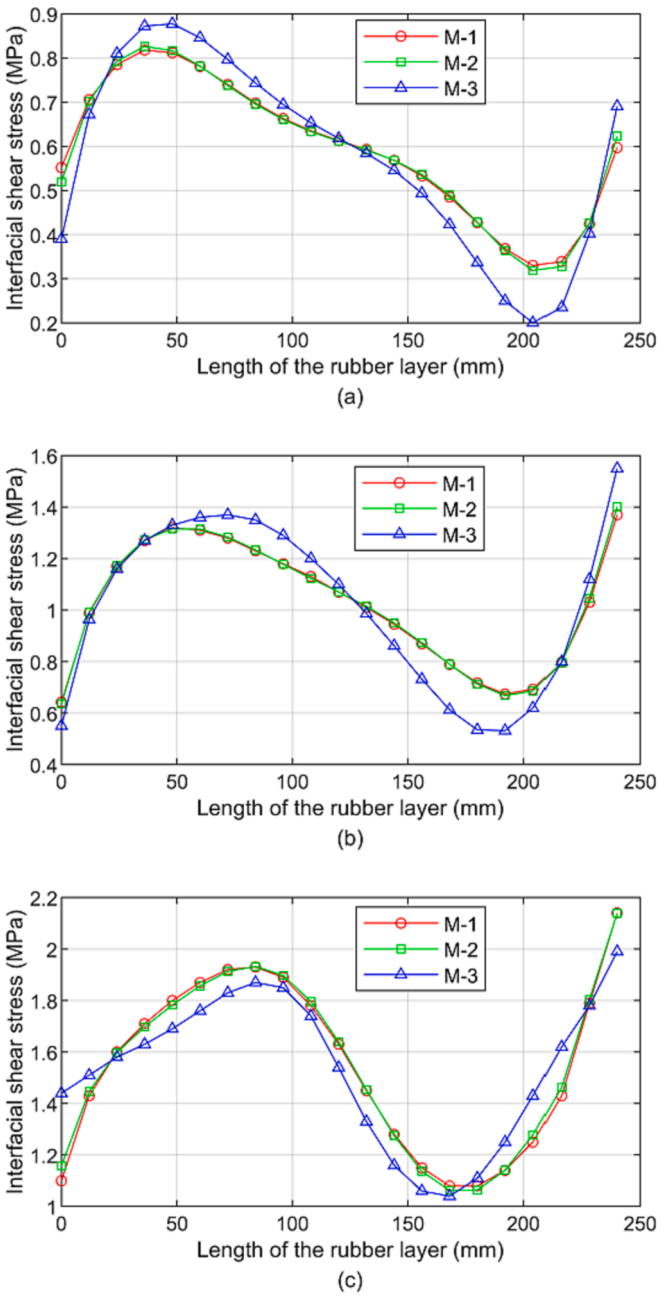

Fig. 37. Distributions of interfacial shear stresses of the first rubber layer under 5 MPa-(a) 100 %γ, (b) 200 %γ, and (c) 300 %γ.

correlation tests, compressive stress correlation tests and loading frequency correlation tests. It could be concluded that the horizontal equivalent stiffness of the FRP seismic isolator was 0.7 kN/mm, the vertical stiffness was 394.3 kN/mm, the maximum allowable vertical compressive stress was defined as 10 MPa, and the ultimate strain could reach 300 % total rubber thickness. The following conclusions were drawn: I The horizontal equivalent stiffness is not so much affected by shear strain variation. Either at 5 MPa or 10 MPa compressive stress, the change in horizontal equivalent stiffness from 100 % to 300 % of shear strain is within 20 %. II Compared with the compressive stress of 5 MPa, the horizontal equivalent stiffness under 10 MPa was reduced by about 10 %, which is an acceptable range, and the horizontal equivalent stiffness decreased significantly under 15 MPa with a decrease of 20–30 %. III The effect of loading frequency on the horizontal equivalent stiffness of the FRP seismic isolator was insignificant. When the horizontal force loading frequency increased from 0.01 Hz to 0.05 Hz, the horizontal equivalent stiffness of the FRP seismic isolator increased by 6.1 %.

Moreover, the mechanical properties of the FRP seismic isolators were further explored through numerical simulations. The results of the numerical model were compared with experimental data to verify the reliability of the numerical model. Numerical simulations were performed to investigate the stress distribution and values inside the FRP isolator. It could be concluded that: I The peak horizontal tensile stress appears in the middle of the first layer FRP plate under the 5 MPa-100 % shear strain and moves to the right along the plate length as the shear strain increases. The increase of peak horizontal tensile stress of the first plate layer is more significant than that of other plate layers with the increase of shear strain. II The vertical normal stress increases with the increase of shear strain. The vertical normal stress positions were kept in the center of the middle layer. III The peak interfacial shear stress in each layer increases with the increase of shear strain. The peak interfacial shear stress under the shear strain of 100 % is at 1/5 of the plate length from the end of the layer near the connecting plate. As the increase of shear strain, the peak interfacial shear stress of the middle layer end became the new peak point position.

Furthermore, the effects of the plane size on the isolator performance has been studied. It could be concluded that:I The horizontal normal stress distributions are similar for square and rectangular isolators. The horizontal normal stresses of both isolators are concentrated in the obtuse angle regions of the bearing section. The peak horizontal tensile stress of the square isolator increases more significantly than that of the rectangular isolator with the increase of shear strain. II The tensile and compressive areas of the rectangle isolator are larger than those of the square isolator, and the stress distribution of the rectangular isolator is more uniform. The peak vertical compressive and tensile stress of the square isolator increases more significantly than that of the rectangular isolator with the increase of shear strain. III The peak interfacial shear stress of the FRP seismic isolator is not significantly affected by the isolator plane size. IV The increase of FRP seismic isolator plane size reduced the internal unbalance torque of isolators and weakened the P-Δ effects. The greater the shear strain, the more pronounced the decline.

Last but not the least, the effect of the P/RTR on the isolator performance has been studied. It could be concluded that:I The increase in P/RTR would reduce the peak value of the horizontal tensile stress, and the P/RTR did not affect the distribution of the horizontal stress. II The peak vertical normal stress was increased by increasing the thickness of the rubber layer. The vertical stress distribution of the plate is the same when the rubber layers' thickness are the same. III The peak interfacial shear stress is only related to rubber thickness, not to plate thickness. The peak interfacial shear stress increased with increasing rubber thickness under the shear strains of 100 % and 200 %, and the peak interfacial shear stress decreased with increasing rubber thickness under the shear strain of 300 %. The interfacial shear stress distribution is the same when the thickness of the rubber layer is the same.

From the results of experimental studies and numerical simulations, it can be seen that the proposed FRP seismic isolator has stable mechanical properties. The proposed FRP seismic isolator can provide sufficient vertical stiffness and load-bearing capacity, while having good deformation capability to provide seismic isolation. The experiments and numerical simulations also showed that the proposed FRP seismic isolator did not exhibit buckling instability and tearing between the plate and rubber under 15 MPa-200 % shear strain and 10 MPa 300 % shear strain. Therefore, the FRP seismic isolator developed in this paper has great engineering application value. In future studies, the application of seismic isolation bearings in actual engineering structures will be studied. The seismic response and seismic isolation effect of the isolated structure will be investigated by numerical simulation and shaking table tests. The economics of FRP seismic isolators compared to steel-rubber seismic isolators will also be analyzed.

CRediT authorship contribution statement

Hao Wang: . **Haoran Mu:** Writing – original draft. **Xiaoxia Guo:** . **Yunfei Zhang:** . **Haowei Ji:** Software, Validation. **Chao Luo:** Writing – review & editing. **Huaiping Feng:** Supervision. **Donglin Liu:** .

Declaration of Competing Interest

The authors declare that they have no known competing financial interests or personal relationships that could have appeared to influence the work reported in this paper.

Data availability

No data was used for the research described in the article.

Acknowledgments

This study was funded by the independent projects for State Key Laboratory of Mechanical Behavior and System Safety of Traffic Engineering Structures [grant number ZZ2021-03]; the Natural Science Foundation of Hebei Province (CN) [grant number E2019210245, E202210095]; S&T Program of Hebei (CN) [grant number 21375407D].

References

[1] Beirami Shahabi A, Zamani Ahari G, Barghian M. Base isolation systems–A state of the art review according to their mechanism. J Rehab Civ Eng 2020;8(2):37–61.
[2] Lupășteanu V, Soveja L, Lupășteanu R, Chingălată C. Installation of a base isolation system made of friction pendulum sliding isolators in a historic masonry orthodox church. Eng Struct 2019;188:369–81.
[3] Lu L-Y, Huang H-W, Wu Y, Wang S-J. Theory and experimental verification of a double sliding isolator with variable curvature. Eng Struct 2021;238:112265.
[4] Tsiavos A, Alexander NA, Diambra A, Ibraim E, Vardanega PJ, Gonzalez-Buelga A, et al. A sand-rubber deformable granular layer as a low-cost seismic isolation strategy in developing countries: experimental investigation. Soil Dyn Earthquake Eng 2019;125:105731.
[5] Ali A, Zhang C, Bibi T, Zhu L, Cao L, Li C, et al. Investigation of five different low-cost locally available isolation layer materials used in sliding base isolation systems. Soil Dyn Earthquake Eng 2022;154:107127.
[6] Froli M, Giresini L, Laccone F. Dynamics of a new seismic isolation device based on tribological smooth rocking (TROCKSISD). Eng Struct 2019;193:154–69.
[7] Cheng C, Chao C. Seismic behavior of rocking base-isolated structures. Eng Struct 2017;139:46–58.
[8] Van Engelen NC. Fiber-reinforced elastomeric isolators: a review. Soil Dyn Earthquake Eng 2019;125:105621.
[9] Kelly JM. Analysis of fiber-reinforced elastomeric isolators. J Seismol Earthquake Eng 1999;44(3):1–8.
[10] Tsai H, Kelly JM. Buckling of short beams with warping effect included. Int J Solids Struct 2005;42(1):239–53.
[11] Tsai H. Compression stiffness of infinite-strip bearings of laminated elastic material interleaving with flexible reinforcements. Int J Solids Struct 2004;41(24):6647–60.
[12] Angeli P, Russo G, Paschini A. Carbon fiber-reinforced rectangular isolators with compressible elastomer: Analytical solution for compression and bending. Int J Solids Struct 2013;50(22–23):3519–27.
[13] Li H, Tian S, Dang X, Yuan W, Wei K. Performance of steel mesh reinforced elastomeric isolation bearing: experimental study. Constr Build Mater 2016;121:60–8.
[14] Mordini A, Strauss A. An innovative earthquake isolation system using fibre reinforced rubber bearings. Eng Struct 2008;30(10):2739–51.
[15] Russo G, Pauletta M, Cortesia A. A study on experimental shear behavior of fiber-reinforced elastomeric isolators with various fiber layouts, elastomers and aging conditions. Eng Struct 2013;52:422–33.
[16] Tan P, Xu K, Wang B, Chang C, Liu H, Zhou FuLin. Development and performance evaluation of an innovative low-cost seismic isolator. Sci China Technol Sci 2014;57(10):2050–61.
[17] Toopchi-Nezhad H, Tait MJ, Drysdale RG. Bonded versus unbonded strip fiber reinforced elastomeric isolators: finite element analysis. Compos Struct 2011;93(2):850–9.
[18] Habieb AB, Valente M, Milani G. Implementation of a simple novel Abaqus user element to predict the behavior of unbonded fiber reinforced elastomeric isolators in macro-scale computations. Bull Earthq Eng 2019;17(5):2741–66.
[19] Habieb AB, Valente M, Milani G. Hybrid seismic base isolation of a historical masonry church using unbonded fiber reinforced elastomeric isolators and shape memory alloy wires. Eng Struct 2019;196:109281.
[20] Habieb AB, Valente M, Milani G. Base seismic isolation of a historical masonry church using fiber reinforced elastomeric isolators. Soil Dyn Earthquake Eng 2019;120:127–45.
[21] Van Engelen NC, Osgooei PM, Tait MJ, Konstantinidis D. Partially bonded fiber-reinforced elastomeric isolators (PB-FREIs). Struct Control Health Monitor 2015;22(3):417–32.
[22] Moon B-Y, Kang G-J, Kang B-S, Kelly JM. Design and manufacturing of fiber reinforced elastomeric isolator for seismic isolation. J Mater Process Technol 2002;130-131:145–50.
[23] GB/T 2567-2008. Test methods for properties of resin casting body. Beijing: Standards Press of China, 2008 (in Chinese).
[24] Xu K, Tan P, Wang B, et al. Comparative study on test performance of two new simple seismic isolation bearings. Earthquake Eng Eng Vib 2014;34(06):11–8.
[25] Kelly JM, Konstantinidis DA, editors. Mechanics of Rubber Bearings for Seismic and Vibration Isolation. Wiley; 2011.
[26] Kalfas KN, Mitoulis SA. Performance of steel-laminated rubber bearings subjected to combinations of axial loads and shear strains. Procedia Eng 2017;199:2979–84.
[27] Kalfas KN, Mitoulis SA, Katakalos K. Numerical study on the response of steel-laminated elastomeric bearings subjected to variable axial loads and development of local tensile stresses. Eng Struct 2017;134:346–57.
[28] Kalfas KN, Mitoulis SA, Konstantinidis D. Influence of steel reinforcement on the performance of elastomeric bearings. J Struct Eng 2020;146(10):4020195.
[29] Zhao Z, Wang Y, Hu X, Weng D. Seismic performance upgrading of containment structures using a negative-stiffness amplification system. Eng Struct 2022;262:114394.